

Microstructural characterization and microstructural effects on the thermal conductivity of AlN(Y₂O₃) ceramics

Ying-Da Yu^a, Aase Marie Hundere^b, Ragnvald Høier^a,
Rafal E. Dunin-Borkowski^c, Mari-Ann Einarsrud^{d,*}

^a*Department of Physics, Norwegian University of Science and Technology, N-7491 Trondheim, Norway*

^b*Elkem Refractories, Torshov, N-0402 Oslo, Norway*

^c*Department of Materials, Parks Road, Oxford OX1 3PH, UK*

^d*Department of Chemistry, Norwegian University of Science and Technology, N-7491 Trondheim, Norway*

Received 28 October 2000; accepted 23 February 2001

Abstract

Two different high density aluminum nitride (AlN) ceramic materials with Y₂O₃ as a sintering additive have been sintered at 1880°C, and characterized using transmission electron microscopy (TEM) and scanning electron microscopy (SEM). The lattice dissolved oxygen content, grain size and amount of secondary phase were fairly similar for the two materials, however, the thermal conductivity was quite different. SEM and TEM studies show that the secondary phase distribution along the grain boundaries or at grain junctions may have a major influence on the thermal conductivity. Microstructural changes were found to disrupt the connection between the high thermal conductivity AlN grains, resulting in a decrease in the thermal conductivity of the material as a whole. No amorphous layer was observed by high resolution transmission electron microscopy (HRTEM) at the cleanest grain boundaries in any of the materials. © 2001 Elsevier Science Ltd. All rights reserved.

Keywords: AlN; Grain boundaries; Sintering; Thermal conductivity

1. Introduction

Aluminum nitride (AlN) has a unique combination of physical properties,¹ and its high thermal conductivity has attracted much attention due to its potential as substrate material for microelectronics. In particular, the intrinsic thermal conductivity of pure AlN single crystals has been calculated to be 300 W/m K at room temperature.² However, because of the high degree of covalent bonding in AlN, complete densification of the material is difficult and liquid phase sintering is necessary. The room temperature thermal conductivity of polycrystalline AlN materials, prepared by liquid-phase sintering, are reported to be in the range 100–260 W/m K.^{3,4} This significant reduction in thermal conductivity is caused by the presence of oxygen impurities.^{2,5,6}

It has been shown that the thermal conductivity of AlN is inversely proportional to the oxygen content dissolved in the AlN lattice.² However, for a given oxygen content, the effect of the morphology of secondary phases in the sintered AlN microstructure can also influence the thermal conductivity considerably.^{7–9}

In a previous study,¹⁰ a series of high density AlN ceramics was produced by using Y₂O₃ as sintering additive. The oxygen content and thermal conductivity were measured, and a general trend of a decreasing thermal conductivity with increasing lattice-dissolved oxygen was observed. However, some samples showed only a small dependence on oxygen content and had higher thermal conductivities than expected. In the present work, two selected AlN materials that have similar lattice oxygen contents and total oxygen content in the same range, but quite different thermal conductivities will be studied. The goal of this paper is to obtain a careful microstructural characterization to understand the effect of grain boundaries and secondary phase distributions on the thermal conductivity of the investigated materials.

* Corresponding author. Tel.: +47-73-594002; fax: +47-73-890860.
E-mail address: mari-ann.einarsrud@chembio.ntnu.no
(M.-A. Einarsrud).

2. Experimental procedure

Commercially available AlN powder (Tokuyama Soda, grade F) containing 0.98 wt.% (0.4 wt.% lattice-dissolved) oxygen and with a specific surface area of 3.4 m²/g, and Y₂O₃ powder (Hermann Starck, Finest) were used as starting materials. Green-bodies with 0.8 wt.% Y₂O₃ (Sample A) and 3.9 wt.% Y₂O₃ (Sample B) were made by slip casting using Alkasurf (Alkaril Chemicals) as a dispersant and isopropanol as a solvent. For Sample A, a BN crucible covered by a BN lid was used during the sintering while for Sample B an open graphite crucible was used to facilitate evaporation.¹¹ Both samples were embedded in an AlN powder bed (grain size < 15 μm) during the sintering, which was performed in a graphite furnace under nitrogen atmosphere (< 5 ppm O₂) at 1880°C for 2 h (see Table 1). The thermal conductivity of the samples was measured using a laser flash method, with a CO₂ laser (Tac2, 215G), to an estimated accuracy of 10%. The lattice-dissolved oxygen content and the total oxygen content of each sample were measured by a selective hot gas extraction method using a LECO TC 436 analyzer, following a method developed by Thomas and Müller.¹²

The identification of secondary phases was performed by using a Philips X-ray diffractometer (XRD) with CuK_α radiation. Fracture surfaces of the samples were investigated by scanning electron microscopy (Zeiss SEM). Transmission electron microscopy studies were performed using a Philips CM30 TEM, and a 300-kV field-emission gun microscope (JEM-3000F).¹³ The specimens were prepared by cutting the as-sintered samples into slices, and then into 3 mm diameter disks using an ultrasonic disc-cutter and subsequently thinned by Argon ion beam milling with a beam energy of 4 kV. In order to observe HRTEM images of grain boundaries, the specimens were tilted to align each grain boundary as “edge-on” and to align adjacent grains to low index zone axes using the procedures described by Clarke.¹⁴ The HRTEM images were acquired digitally in a 1 k × 1 k Gatan CCD camera.

3. Results

Table 1 lists the measured thermal conductivity, mean grain size and oxygen content of each sample. As shown in the table, both Sample A and B have about similar

lattice dissolved oxygen contents, but their corresponding thermal conductivities are quite different. Both samples obtained a density close to theoretical.

The microstructures of the two samples were first investigated by SEM. Back-scattered SEM micrographs of surfaces from Sample A and B are shown in Fig. 1(a) and (b), respectively. Yttrium–aluminate secondary phases exhibit bright contrast in the figures. In Sample A, the yttrium–aluminate secondary phases are formed along the AlN grain boundaries. In Sample B, the yttrium–aluminate secondary phases are primarily dispersed at the isolated AlN grain junctions. Similar microstructures are also typically observed in the corresponding low magnification TEM micrographs as shown in Fig. 2(a) and (b). Here, the yttrium–aluminate secondary phases (marked with arrows) exhibit dark contrast.

Yttrium–aluminum garnet (YAG) was found by XRD to be the major secondary phase in the bulk of both samples. However, on the surface of the samples, YAG was observed on Sample A while the more yttrium rich phases, yttrium–aluminum perovskite (YAP), yttrium–aluminum monoclinic (YAM) and Y₂O₃ were found on Sample B.

In order to understand the interface between the secondary phase and the AlN matrix, HRTEM studies were performed with the Philips CM30 TEM. Fig. 3(a) shows a low-magnification TEM micrograph of the YAP secondary phase in Sample B. A HRTEM image, obtained from the double arrow region in Fig. 3(a) taken along the YAP [111] orientation, is shown in Fig 3(b). It is clearly shown that an amorphous layer with thickness of about 5 nm exists between the secondary phase and the adjacent AlN matrix.

The AlN grain boundary structure in Samples A and B was investigated using the JEM-3000F TEM, with the incident beam parallel to the grain boundary and the adjacent grains close to low index zone axes. Fig. 4(a) shows a HRTEM image of a representative vertical grain boundary in Sample A. The upper grain orientation is close to the AlN [001] (AlN, hexagonal, *a* = 0.3111 nm, *c* = 0.498 nm) and with the AlN (101) fringes visible in the lower grain. Fig. 4(b) shows a representative HRTEM image of a vertical grain boundary in Sample B, in which the lower grain is close to the AlN [1–10] orientation and the AlN (100) fringes are visible in the upper grain. None of the grain boundaries has observed an amorphous layer in the HRTEM micrographs. However, EDS spectra obtained using a 0.6 nm probe indicated

Table 1
Experimental details and selected properties of AlN samples

Sample code	Wt.% Y ₂ O ₃	Sintering condition	Thermal cond. (W/mK)	Lattice oxygen content (wt.%)	Total oxygen content (wt.%)	Grain size (μm)
A	0.8	BN crucible	91	0.56	1.32	3.4
B	3.9	C crucible	154	0.52	1.63	2.9

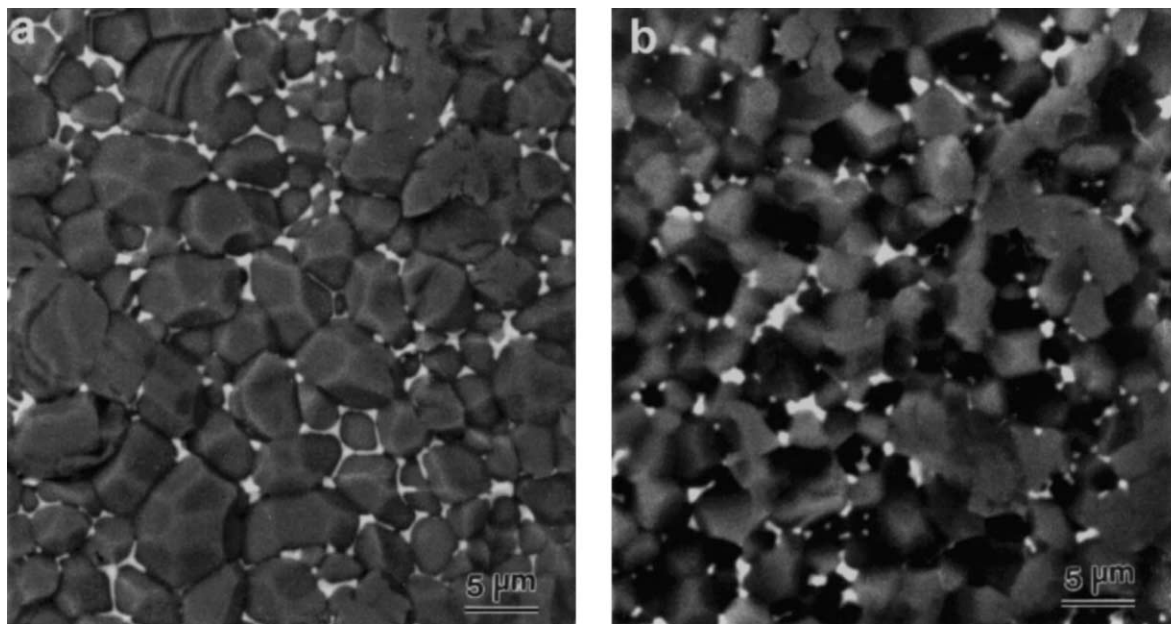


Fig. 1. Back-scatter SEM micrographs. (a) Sample A, showing yttrium–aluminate secondary phases along AlN grain boundaries; (b) Sample B, showing yttrium–aluminate secondary phases at isolated AlN grain junctions.

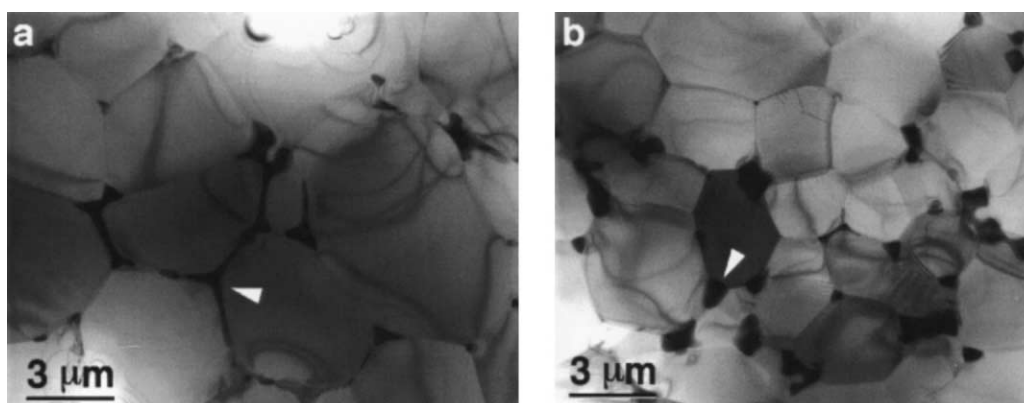


Fig. 2. Low magnification TEM bright-field images of (a) Sample A (arrow shows dark secondary phase contrast formed along AlN boundaries), and (b) Sample B (arrow shows secondary phase contrast at isolated AlN grain junctions).

that both boundaries have higher yttrium and oxygen contents than the adjacent grains. Two representative EDS spectra obtained from the AlN grain and the grain boundary in Fig. 4(b) are shown in Fig. 5(a) and (b), respectively.

4. Discussion

Assuming no weight loss during sintering, calculations of the compositions of the secondary phases show that Sample A should contain mainly YAG phase with excess of Al_2O_3 after sintering, while Sample B should contain the YAG phase only.¹⁰ During sintering, the reaction



might give a weight loss if evaporation of $\text{Al}_2\text{O(g)}$ or carbo-thermal reduction with CO is allowed to occur.¹⁰ This weight loss will give an enrichment of Y_2O_3 in the secondary phase. An accurate weight loss could not be recorded due to sintering in the powder bed. However, there was a weight loss especially of sample B because a change in the composition of the sample was observed, the yttrium rich phases YAP, YAM and Y_2O_3 were detected on the sample surface, and the total oxygen content had decreased. This sample was the one sintered in the open graphite furnace. To control the weight loss is of great importance for industrial production of AlN ceramics.

Figs. 1 and 2 show that the amounts of secondary phases in the two samples are fairly equal, but the distributions of the secondary phases are quite different. In sample A, the secondary phases are located along several grain boundaries showing good wetting properties of

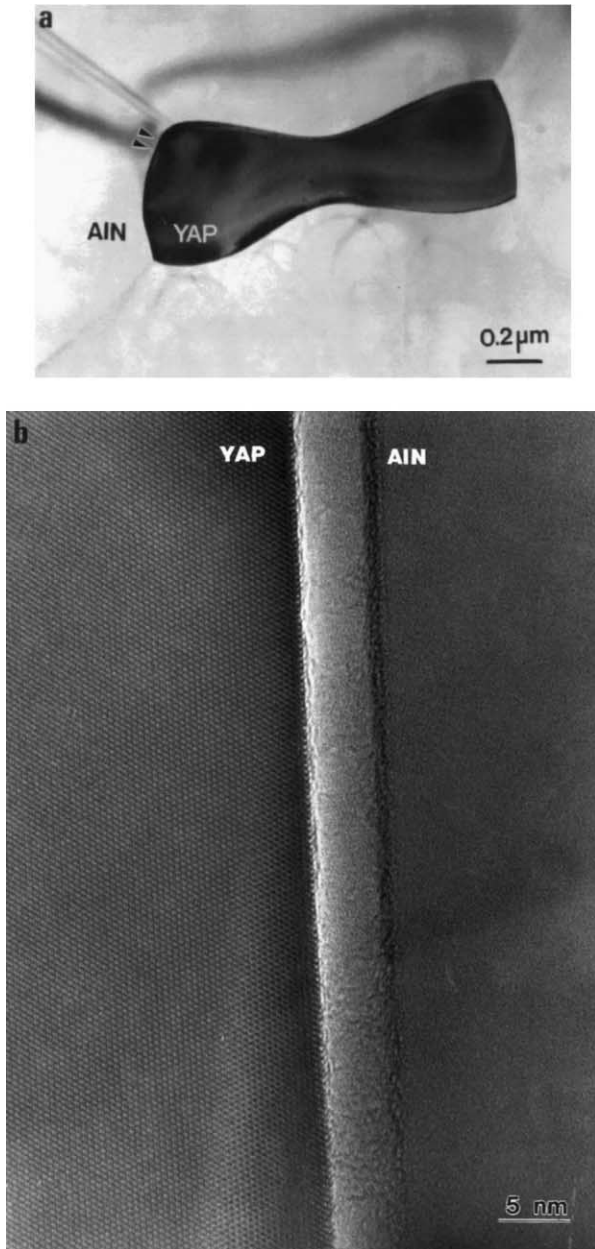


Fig. 3. Thin amorphous layer between secondary phase and AlN matrix in Sample B. (a) Low-magnification TEM bright-field micrograph; (b) HRTEM image obtained along YAP [111] from double arrow region marked in (a).

the liquid during final stage of sintering (assuming no change in wetting properties during cooling). In sample B, however, the secondary phases are located at the triple points and no secondary phase can be seen along the grain boundaries at this magnification. It has previously been shown¹⁵ that the compositions of secondary phases (YAG, YAP or YAM) have only a minor influence on the wetting properties of the secondary phases during sintering. However, it was observed that the wetting was dependent on the content of oxygen impurities on the AlN grain boundaries. Low oxygen containing grain boundaries were observed performing the sintering in

the open graphic crucible or adding small amounts of carbon to the sample. We therefore propose that the main reason for the different microstructures observed, is the different sintering conditions used. Sintering in an open crucible allowing reaction (1) and possible carbo-thermal reduction with CO¹⁰ to occur induces a driving force for segregation of the secondary phases to the isolated triple points.

Since the lattice oxygen content, grain size, and total amount of secondary phases in the two materials are fairly similar, we suggest that the distribution of secondary phases in the two materials was most likely the main reason for the observed difference in thermal conductivity. The presence of secondary phases along the AlN grain boundaries disrupts the connections between high thermal conductivity AlN grains. This is due to the fact that the thermal conductivity of the secondary phases is low, i.e. YAG only 11 W/m K.¹⁶ In addition, the thin amorphous layer between the secondary phase and the AlN matrix, such as that shown in Fig. 3(b), will further reduce the thermal conductivity.

The HRTEM results, however, show little difference between the grain boundary structures of the observed cleanest grain boundaries in the two samples (Fig. 4). The fact that Sample A shows lower thermal conductivity even though its grain boundaries contain little secondary phase such as shown in Fig. 4(a) suggests that such boundaries do not form continuous paths for thermal conduction through the whole sample. However, it is interesting to note that quite clean grain boundaries are present in both samples. By using the model proposed by Buhr and Müller¹⁷ for calculation of the effect of an amorphous layer on the thermal conductivity, only a very small effect on thermal conductivity is expected from the cleanest grain boundaries with the present oxygen contents.

The small enhancement in yttrium and oxygen at the grain boundaries in both samples [Fig. 5(b)] may be associated with the presence of some amorphous or disordered material, despite their apparently crystalline form of the boundaries in Fig. 4. Keblinski et al.¹⁸ have used molecular-dynamics simulations to investigate the thin amorphous films commonly found at high-energy grain boundaries in covalent polycrystalline ceramics. The present observations could be explained in part by a lack of contrast between amorphous and crystalline regions, as pointed by Cahn,¹⁹ and in part by the strong defocus-dependent delocalisation of the lattice fringe contrast visible at such boundaries.

The presence of defects such as inversion domain boundaries (IDBs)²⁰ would also affect the thermal conductivity of AlN by acting as oxygen-gathering defects that remove oxygen from large parts of the bulk grains. However, the present TEM observations show no obvious difference in defect density between the two samples examined here.

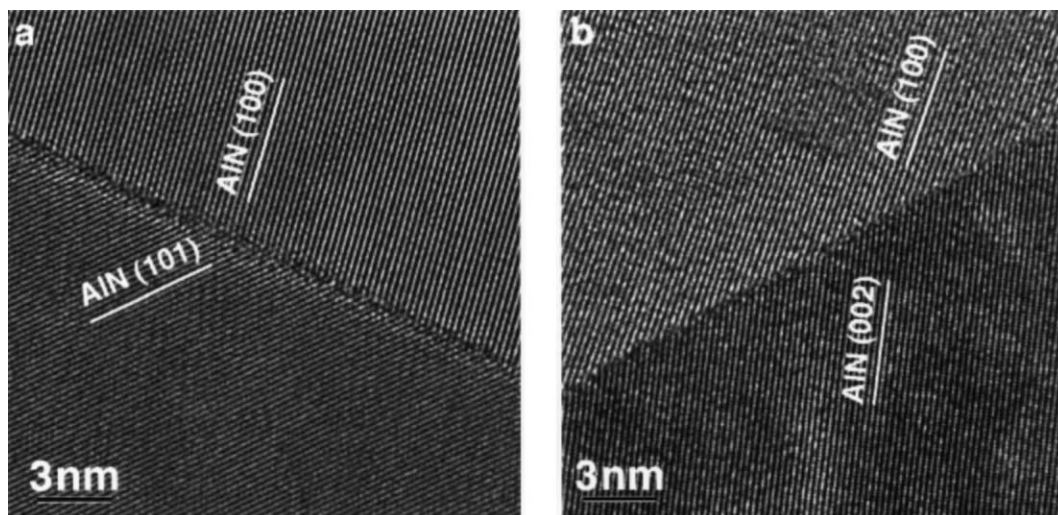


Fig. 4. Representative HRTEM images of vertical AlN grain boundaries, with AlN grains close to low index planes. (a) Sample A; (b) Sample B.

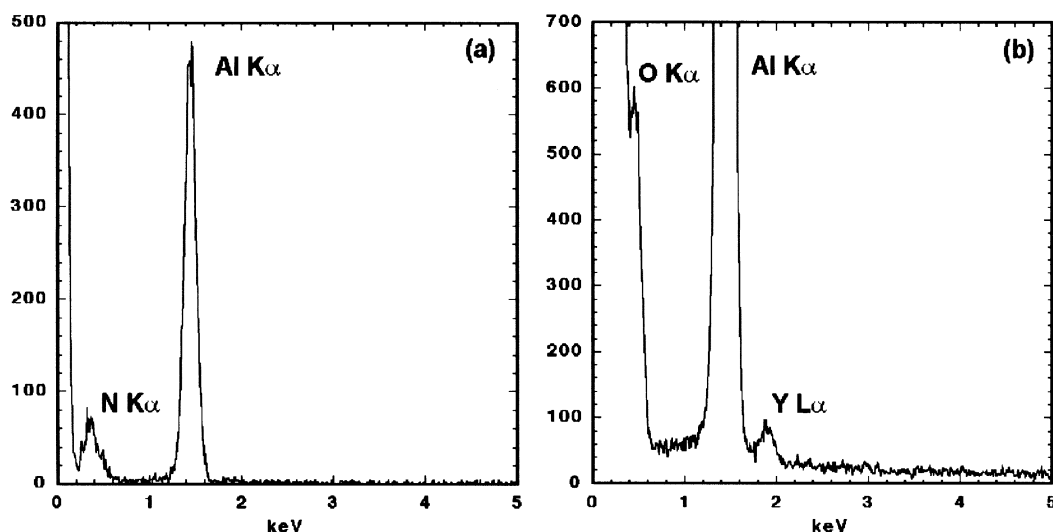


Fig. 5. EDS spectra obtained using 0.6 nm probe from area shown in Fig. 4(b). (a) AlN grain; (b) grain boundary.

Even though the present EDS results imply that thin amorphous films still possibly exist at the grain boundaries, the grain boundary states in both samples (Fig. 4) are much cleaner than that in other similar ceramic systems, such as for Si_3N_4 system, where the amorphous films around 1.0 nm thick were present at almost all Si_3N_4 grain boundaries.²¹

5. Conclusions

SEM and TEM observations have shown that the presence of secondary phases along grain boundaries or at grain junctions has a major influence on the thermal conductivity of AlN materials. Microstructural changes were found to disrupt the connection between the AlN grains, resulting in a decrease in the thermal conductivity

of the materials. No amorphous layer was observed by HRTEM at the cleanest grain boundaries, however, the presence of yttrium and oxygen were confirmed by EDS. HRTEM images confirmed the presence of an amorphous layer on the boundary between the secondary phase and the AlN matrix. No substantial differences were observed between the cleanest AlN grain boundaries in the two materials, suggesting that the structure of the cleanest AlN grain boundaries is not the primary origin of the difference in thermal conductivity between the two investigated samples.

Acknowledgements

The authors thank the Norwegian Research Council for financial support and Dr. J.L. Hutchison for the use of the Jeol JEM-3000F in Oxford.

References

1. Trampert, A., Brandt, O. and Ploog, K. H., Crystal structure of group III nitrides. In *Semiconductors and Semimetals*, Vol. 50, ed. J. I. Pankove and T. D. Moustakas. Academic Press, New York, 1998, pp. 167–192.
2. Slack, G. A., Tanzilli, R. A., Pohl, R. O. and Vandersande, J. W., The intrinsic thermal-conductivity of AlN. *J. Phys. Chem. Solids*, 1987, **48**, 641–647.
3. Haase, I. and Himple, G., Development of single phase aluminum nitride ceramics. *Silicates Ind.*, 1993, **7/8**, 143–148.
4. Ueno, F. and Horiguchi, A., In *Euro-Ceramics*, Vol. 1, ed. G. de With, R. A. Terpstra and R. Metselaar. Elsevier Applied Science, London, 1989, pp. 1383.
5. Watari, K., Ishizaki, K. and Tsuchiya, F., Phonon-scattering and thermal conduction mechanisms of sintered aluminum nitride ceramics. *J. Mater. Sci.*, 1993, **28**, 3709–3714.
6. Watari, K., Ishizaki, K. and Fujikawa, T., Thermal conduction mechanism of aluminum nitride ceramics. *J. Mater. Sci.*, 1992, **27**, 2627–2630.
7. Kurokawa, Y., Utsumi, K. and Takamizawa, H., Development and microstructural characterization of high-thermal-conductivity aluminum nitride ceramics. *J. Am. Ceram. Soc.*, 1988, **71**, 588–594.
8. Yoneda, Y., Takaoka, T., Takeshima, Y., Sakabe, Y., Kasamani, T. and Wakino, K. Preparation of high thermal conductivity AlN ceramics and metallisation. In *IMC Proceed., Tokyo*, 1988, pp. 147–152.
9. Ruckmich, S., Kranzmaann, A., Bischoff, E. and Brook, R. J., A description of microstructure applied to the thermal conductivity of aluminium nitride ceramics. *J. Eur. Ceram. Soc.*, 1991, **7**, 335–341.
10. Hundere, A. M., *Sintering of Aluminum Nitride (AlN) Ceramics*. PhD thesis, Norwegian Institute of Technology, Trondheim, Norway, 1995.
11. Hundere, A. M. and Einarsrud, M.-A., Effects of reduction of the Al–Y–O containing secondary phases during sintering of AlN with YF₃ additions. *J. Eur. Ceram. Soc.*, 1996, **16**, 899–906.
12. Thomas, A. and Müller, G., Determination of the concentration of oxygen dissolved in the AlN lattice by hot gas extraction from AlN ceramics. *J. Eur. Ceram. Soc.*, 1991, **8**, 11–19.
13. Hutchison, J. L., Doole, R. C., Dunin-Borkowski, R. E., Sloan, J. and Green, M. L. H., The development and assessment of a high performance field-emission-gun analytical HRTEM for materials science applications. *JEOL News*, 1999, **34E**, 10–15.
14. Clarke, D. R., On the detection of thin intergranular films by electron microscopy. *Ultramicroscopy*, 1979, **4**, 33–44.
15. Hundere, A. M. and Einarsrud, M.-A., Microstructure development in AlN(YF₃) ceramics. *J. Eur. Ceram. Soc.*, 1997, **17**, 873–878.
16. Klein, P. H. and Croft, W. J., Thermal conductivity, diffusivity, and expansion of Y₂O₃, Y₃Al₅O₁₂, and LaF₃ in the range of 77–300 K. *J. Appl. Phys.*, 1967, **38**, 1603–1607.
17. Buhr, H. and Müller, G., Microstructure and thermal conductivity of AlN(Y₂O₃) ceramics sintered in different atmospheres. *J. Eur. Ceram. Soc.*, 1993, **12**, 271.
18. Keblinski, P., Phillpot, S. R., Wolf, D. and Gleiter, H., On the thermodynamic stability of amorphous intergranular films in covalent materials. *J. Eur. Ceram. Soc.*, 1997, **80**, 717–732.
19. Cahn, R. W., Materials science — silicon self-analysis. *Nature*, 1997, **390**, 334.
20. Westwood, A. D., Youngman, R. A., McCartney, M. R., Cormack, A. N. and Notis, M. R., Oxygen incorporation in aluminum nitride via extended defects: Part I. Refinement of the structural model for the planar inversion domain boundary. *J. Mater. Res.*, 1995, **10**, 1270–1286.
21. Riley, F. L., Silicon nitride and related materials. *J. Am. Ceram. Soc.*, 2000, **83**, 245–265.